Optics Letters

Dispersion engineering of hyperbolic plasmons in bilayer 2D materials

Maturi Renuka,[1] Xiao Lin,[2] Zuojia Wang,[3,*] Lian Shen,[1] Bin Zheng,[1] Huaping Wang,[1] and Hongsheng Chen[1]

[1]Key Laboratory of Advanced Micro/Nano Electronic Devices & Smart Systems of Zhejiang, College of Information Science and Electronic Engineering, Zhejiang University, Hangzhou 310027, China
[2]Division of Physics and Applied Physics, School of Physical & Mathematical Sciences, Nanyang Technological University, Singapore 637371, Singapore
[3]School of Information Science and Engineering, Shandong University, Qingdao 266237, China
*Corresponding author: z.wang@sdu.edu.cn

Received 8 October 2018; revised 24 October 2018; accepted 25 October 2018; posted 29 October 2018 (Doc. ID 346675); published 21 November 2018

Recent progress on anisotropic 2D materials brings new technologies for directional guidance of hyperbolic plasmons. Here, we investigate the plasmonic modes in twisted bilayer 2D materials (e.g., black phosphorous). Calculated dispersion curves show that two hyperbolas split as the twisted angle increases. The topological transition from closed ellipses to open hyperbolas is achieved by varying the frequency, indicating switching between highly directional and omnidirectional plasmons. These findings will provide potential applications of anisotropic 2D materials in the design of tunable field effect transistors and waveguides.

https://doi.org/10.1364/OL.43.005737

Highly squeezed polaritons, including plasmon polaritons in graphene [1] and phonon polaritons in hexagonal boron nitride [2], in natural materials, and Dyakonov plasmons [3,4] on hyperbolic metamaterial in artificial materials with a wide range of varying bandgaps from optical [5] to mid-IR [6,7] range, have been a growing area of research. The deep subwavelength confinement of light, with $\lambda_0/\lambda_{spp} > 100$, facilitates controlling light at nanoscale, leading to unique applications, including negative refraction [2,8], subdiffraction focusing [9], sensing [10], superscattering [11], separating the Doppler effect from the superlight inverse Doppler effect [12], and nanophotonics circuits [13]. There are many types of highly squeezed polaritons, which include isotropic polaritons in graphene, hexagonal boron nitride, hyperbolic polaritons in black phosphorous [5], and metal dichalcogenides and trichalcogenides [14]. However, hyperbolic polaritons have a distinct property to enhance the directional propagation of the wave, which is central for development of on-chip devices. These hyperbolic materials have potential application in the directional guidance of energy [15,16], hyperlensing [17], subwavelength focusing [18], electronics, and optoelectronics [19,20]. Recently, there have been comprehensive investigations of anisotropic plasmons on bilayer and multilayer systems due to their few potential applications, such as field effect transistors [21–24], waveguides [25], and photodetectors tuned by field effects [26]. Furthermore, bilayer and multilayer systems show some interesting properties due to coupling between layers and provide an additional tuning parameter, i.e., relative angular orientation to modify the dispersion curve [27–30]. However, the effect of tuning parameter on a bilayer hyperbolic material has not been explored. In this Letter, we examine the effect of the change in relative orientation and chemical potential on plasmon modes in a bilayer hyperbolic material based on 2D materials. We reveal that the propagation of surface plasmons along a desired direction can be efficiently tuned by changing relative orientation along the same direction between the layers. We observe that the shape of the dispersion curve is modified by increasing the chemical potential of layers, and the change in shape of the curve from elliptical to hyperbolic at the topological transition point.

In general, a 2D anisotropic monolayer supports hybrid modes [31,32], which are the superpositions of TE and TM modes. But the fraction of TE mode in a hybrid mode for a hyperbolic material is very small compared to hybrid mode in anisotropic materials [33,34]. Therefore, we obtain the condition for the existence of TM plasmonic modes from the dispersion relation of a bilayer system. The 2D bilayer system consists of two monolayers with surface conductivities $\overline{\overline{\sigma}}_{3|1}$ and $\overline{\overline{\sigma}}_{1|2}$ of top and bottom layers, respectively. The layers are separated by a dielectric material of thickness $2d$, as shown in Fig. 1(a). The separation between layers is adequate to prevent the modification of optical properties of each layer. The relative lossless permittivities in three regions are given as $\varepsilon_{r3}, \varepsilon_{r1}$, and ε_{r2}, respectively. For TM waves, the magnetic field has a component along only y direction, i.e., H_y. The magnetic field in three regions are assumed to be

Region 3 ($z > d$)

$$H_y = Ae^{i\beta x}e^{-k_{z3}z}, \tag{1}$$

Region 1 ($d < z < -d$)

$$H_y = Ce^{i\beta x}e^{k_{z1}z} + De^{i\beta x}e^{-k_{z1}z}, \tag{2}$$

Region 2 ($z < -d$)

$$H_y = Be^{i\beta x}e^{k_{z2}z}, \tag{3}$$

where ω is the frequency, c is the velocity of light, and $k_{zi} = \sqrt{\beta^2 - \frac{\omega^2}{c^2}\varepsilon_{ri}}(i = 1, 2, 3)$ and β are the components of wave vector perpendicular and parallel to the interface, respectively. The boundary conditions applied are $\vec{z} \times (\vec{E}_1 - \vec{E}_2) = 0$ and $\vec{z} \times (\vec{H}_1 - \vec{H}_2) = \overline{\overline{\sigma}}\vec{E}$, at interface $z = d$ and $z = -d$. The dispersion equation of the bilayer system is derived using the field distributions in Eqs. (1)–(3) and the boundary conditions

$$\Omega(k_x, k_y) = e^{-4k_{z1}d} - \frac{\left[\frac{k_{z1}}{\varepsilon_{r1}}\left(1 + \frac{i\sigma^b k_{z2}}{\omega\varepsilon_0\varepsilon_{r2}}\right) + \frac{k_{z2}}{\varepsilon_{r2}}\right]\left[\frac{k_{z1}}{\varepsilon_{r1}}\left(1 + \frac{i\sigma^a k_{z3}}{\omega\varepsilon_0\varepsilon_{r3}}\right) + \frac{k_{z3}}{\varepsilon_{r3}}\right]}{\left[\frac{k_{z1}}{\varepsilon_{r1}}\left(1 + \frac{i\sigma^b k_{z2}}{\omega\varepsilon_0\varepsilon_{r2}}\right) - \frac{k_{z2}}{\varepsilon_{r2}}\right]\left[\frac{k_{z1}}{\varepsilon_{r1}}\left(1 + \frac{i\sigma^a k_{z3}}{\omega\varepsilon_0\varepsilon_{r3}}\right) - \frac{k_{z3}}{\varepsilon_{r3}}\right]} = 0, \tag{4}$$

where $2d$ is the distance between the two anisotropic layers, ε_0 is the permittivity of free space, $\sigma^a = \sigma_{3|1,x'x'}\cos^2\varphi + \sigma_{3|1,y'y'}\sin^2\varphi$, $\sigma^b = \sigma_{1|2,x''x''}\cos^2(\varphi+\theta) + \sigma_{1|2,y''y''}\sin^2(\varphi+\theta)$, φ is the angle between axes x and x' and θ is the relative angle between axes x' and x'', $\cos\varphi = k_x/\sqrt{k_x^2 + k_y^2}$ and $\sin\varphi = -k_y/\sqrt{k_x^2 + k_y^2}$, x', y', and x'', y'' specify the in-plane optical axes of surface conductivities for the top and bottom 2D materials, respectively, as shown in Fig. 1(b).

The dispersion relation in Eq. (4) is the sum of two terms; the first term determines the strength of coupling between two layers by varying the distance, and the second term specifies the effect of various other parameters (relative orientation, chemical potential, substrate effects, etc.) on the modes of the system. Equation (4) reduces to a simpler form under the following conditions: (a) if both layers are isotropic $\overline{\overline{\sigma}}_{3|1} = \overline{\overline{\sigma}}_{1|2} = \sigma$ [35],

$$e^{-4k_{z1}d} - \frac{\left[\frac{k_{z1}}{\varepsilon_{r1}}\left(1 + \frac{i\sigma k_{z2}}{\omega\varepsilon_0\varepsilon_{r2}}\right) + \frac{k_{z2}}{\varepsilon_{r2}}\right]\left[\frac{k_{z1}}{\varepsilon_{r1}}\left(1 + \frac{i\sigma k_{z3}}{\omega\varepsilon_0\varepsilon_{r3}}\right) + \frac{k_{z3}}{\varepsilon_{r3}}\right]}{\left[\frac{k_{z1}}{\varepsilon_{r1}}\left(1 + \frac{i\sigma k_{z2}}{\omega\varepsilon_0\varepsilon_{r2}}\right) - \frac{k_{z2}}{\varepsilon_{r2}}\right]\left[\frac{k_{z1}}{\varepsilon_{r1}}\left(1 + \frac{i\sigma k_{z3}}{\omega\varepsilon_0\varepsilon_{r3}}\right) - \frac{k_{z3}}{\varepsilon_{r3}}\right]} = 0, \tag{5}$$

and (b) if the distance between layers becomes large, i.e., $d \to \infty$, the equation simplifies to the dispersion equation of monolayers [36]:

$$\frac{k_{z1}}{\varepsilon_{r1}} + \frac{k_{z2}}{\varepsilon_{r2}} + \frac{i\sigma k_{z2}k_{z1}}{\omega\varepsilon_0\varepsilon_{r2}\varepsilon_{r1}} = 0, \tag{6}$$

$$\frac{k_{z1}}{\varepsilon_{r1}} + \frac{k_{z3}}{\varepsilon_{r3}} + \frac{i\sigma k_{z3}k_{z1}}{\omega\varepsilon_0\varepsilon_{r3}\varepsilon_{r1}} = 0. \tag{7}$$

The surface conductivity of a 2D anisotropic monolayer (e.g., black phosphorous) can be modeled using a minimal model [16]. The surface conductivity $\overline{\overline{\sigma}}$ is the sum of two terms; the first term is due to the intraband transition, and the second term is due to the interband transition in the material:

$$\overline{\overline{\sigma}} = \begin{pmatrix} \sigma_{xx} & 0 \\ 0 & \sigma_{yy} \end{pmatrix}, \tag{8}$$

where

$$\sigma_{jj} = \frac{ie^2}{\omega + i\eta}\frac{n}{m_j} + s_j\left[H(\omega - \omega_j) + \frac{i}{\pi}\ln\left|\frac{\omega - \omega_j}{\omega + \omega_j}\right|\right], \tag{9}$$

and $j = x, y$, where e is the charge of electron, n is the number density of electron, η is a relaxation time, m_j is the mass of electron along jth direction, $H(\omega - \omega_j)$ is the step function, ω_j is the interband transition in material along jth direction, and s_j specifies the strength of the interband transition. In Fig. 2, the imaginary part of surface conductivities for the electron density $n = 3 \times 10^{13}$ cm^{-2}, along x and y directions are plotted [16]. The insets in Fig. 2 represent plasmon modes in anisotropic and hyperbolic 2D monolayers surrounded by air. The real part of conductivities specifies the dissipation in the system.

For the anisotropic material with $\sigma_{xx} = (0.06 + i0.41)mS$ and $\sigma_{yy} = (0.01 + i0.05)mS$ at 15 THz, the mode in k-space has quasi-elliptical shape and is focused along the direction of large imaginary conductivity [15]. The modes in k-space for hyperbolic material with $\sigma_{xx} = (0.01 + i0.29)mS$ and $\sigma_{yy} = (0.002 - i0.29)mS$) at 72 THz have hyperbolic shape [15]. These modes specify the direction of propagation of a plasmon wavefront on the surface of materials. The direction of propagation of plasmon energy in an anisotropic material is given by group velocity, $v_g = \nabla_{\vec{k}}\omega(k)$, which is different from the plasmons in k- surface [37]. Then the energy propagation can be tuned by modification of the plasmons. Here, we discuss how wavefront propagation changes with changes in different parameters such as relative angular orientation and chemical potential.

The dispersion curve for the bilayer system is the solution of Eq. (4). First, we consider the effect of orientation on the dispersion curve. The three regions are assumed to be free

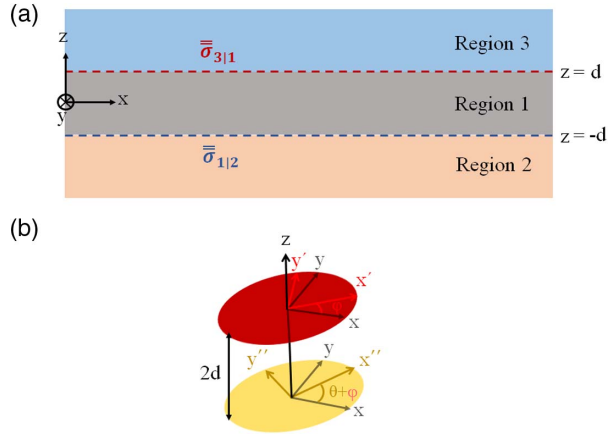

Fig. 1. (a) Schematic structure of a bilayer system with 2D materials. The conductivities of the top and bottom layers are $\overline{\overline{\sigma}}_{3|1}$ and $\overline{\overline{\sigma}}_{1|2}$, respectively. The layers are separated by a dielectric slab of thickness $2d$. (b) Orientation of the principal axes of conductivities in each 2D layer and axis of the bilayer system. The principal axes of conductivities in each 2D layer, x' and x'', with respect to bilayer axis, x, form an angle of φ and $\varphi + \theta$, respectively.

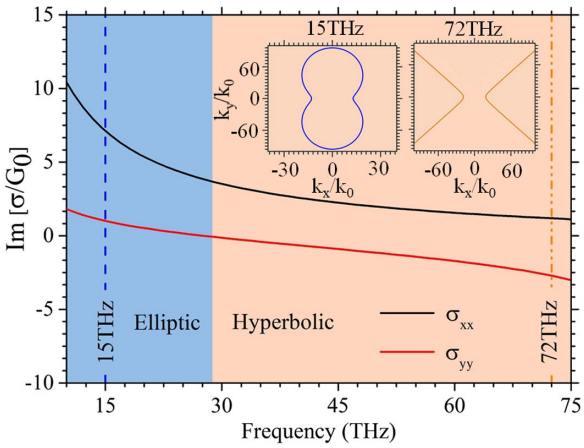

Fig. 2. Imaginary part of conductivities along the principal axes of 2D material for $n = 3 \times 10^{13}$ cm^{-2}, where $G_0 = e^2/4\hbar$. The insets are the plasmonic modes in monolayer 2D materials surrounded by air, for anisotropic material $[\sigma_{xx} = (0.06 + i0.41)mS, \sigma_{yy} = (0.01 + i0.05)mS]$ at an operational frequency of 15 THz and hyperbolic material $[\sigma_{xx} = (0.01 + i0.29)mS, \sigma_{yy} = (0.002 - i0.29)mS]$ at 72 THz.

space, i.e., $\varepsilon_{r1} = \varepsilon_{r2} = \varepsilon_{r3} = 1$, and the distance between two layers is taken to be $2d = 5$ nm. Figures 3(a)–3(d) reveal the dispersion curve for different relative angular orientations varying from $\theta° = 0°$ to 90°, and the conductivities of top and bottom layers are assumed to be the same.

The dispersion curve in Fig. 3(a) has two hyperbolas, which is due to parallel ($\theta° = 0°$) orientation of the two layers with each principal axis along the same direction. As the relative angles increase to 30°, the shape of dispersion curves does not change, but the orientations of two curves relative to each other have also changed by the same angle [Fig. 3(b)]. Similarly, for $\theta° = 60°$, one of the curves is rotated relative to each other by the same angle. At $\theta° = 90°$, the two curves become orthogonal to each other [Fig. 3(d)]. These curves show highly directional and tunable surface plasmon waves with the change in relative

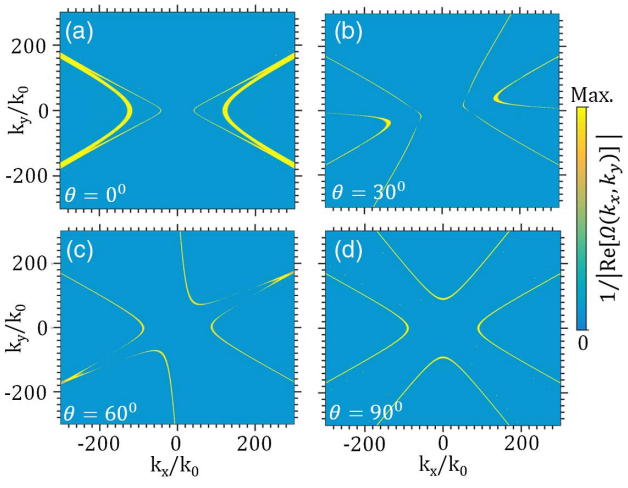

Fig. 3. Plasmon modes in a bilayer system for different relative orientations, θ, between layers: (a) 0°, (b) 30°, (c) 60°, and (d) 90°. The conductivities of the layers are $\sigma_{3|1,x'x'} = \sigma_{1|2,x''x''} = (0.003 + i0.07)mS$ and $\sigma_{3|1,y'y'} = \sigma_{1|2,y''y''} = (0.0006 - i0.16)mS$, and the layer distance is $2d = 5$ nm, $n = 3 \times 10^{13}$ cm^{-2} at 72 THz.

orientation. This could serve as the parameter for directional excitation of energy in the material. This parameter would provide an additional guideline to engineer the directional propagation of waves on the surface of material in a device. Furthermore, if the distance between the two layers increases, then the coupling between the layers vanishes, and the dispersion curve reduces to monolayer dispersion curves.

The effect of a change in chemical potential on the dispersion curve is shown in Figs. 4(a)–4(d). The conductivity changes from $\sigma_{3|1,x'x'} = \sigma_{1|2,x''x''} = (0.003 + i0.07)mS$, $\sigma_{3|1,y'y'} = \sigma_{1|2,y''y''} = (0.0006 - i0.16)mS$, for $n = 3 \times 10^{13}$ cm^{-2}, to $\sigma_{3|1,x'x'} = \sigma_{1|2,x''x''} = (0.01 + i0.29)mS, \sigma_{3|1,y'y'} = \sigma_{1|2,y''y''} = (0.002 - i0.12)mS$, for $n = 10 \times 10^{13}$ cm^{-2} at a fixed frequency 72 THz. The increment in chemical potential leads to an increase in the magnitude of conductivity, which in turn induces change in the shape of the dispersion curve. Furthermore, the curve progressively shifts to the center with the increase in conductivity, as shown in Figs. 4(a) and 4(b). This shifting leads to an overlap of the curve, which in turn influences the splitting of the curves. The splitting introduces a distinct mode at the center. The change in shape of the curve is due to strong coupling between the modes of top and bottom layers.

Figures 5(a)–5(d) show the change in dispersion curve due to transition from elliptical, $\sigma_{3|1,x'x'} = \sigma_{1|2,x''x''} = (0.06 + i0.41)mS, \sigma_{3|1,y'y'} = \sigma_{1|2,y''y''} = (0.01 + i0.05)mS$, to hyperbolic, $\sigma_{3|1,x'x'} = \sigma_{1|2,x''x''} = (0.003 + 0.07)mS, \sigma_{3|1,y'y'} = \sigma_{1|2,y''y''} = (0.0006 - i0.16)mS$), conductivity values. Figure 5(a) shows the dispersion curves due to elliptical conductivity in both layers. As the magnitude of conductivity decreases, the shape of the dispersion curve becomes an elongated ellipse along x and y directions. This allows the coupling of incident waves with low and high wavenumbers [15]. As the

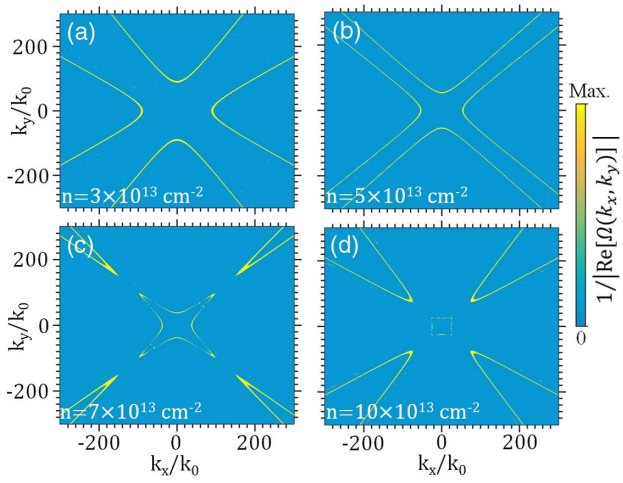

Fig. 4. Effect of a change in chemical potential on plasmonic mode. The conductivity values are: (a) $\sigma_{3|1,x'x'} = \sigma_{1|2,x''x''} = (0.003 + i0.07)mS$ and $\sigma_{3|1,y'y'} = \sigma_{1|2,y''y''} = (0.0006 - i0.16)mS$ for $n = 3 \times 10^{13}$ cm^{-2}, (b) $\sigma_{3|1,x'x'} = \sigma_{1|2,x''x''} = (0.005 + i0.13)mS$ and $\sigma_{3|1,y'y'} = \sigma_{1|2,y''y''} = (0.001 - i0.15)mS$ for $n = 5 \times 10^{13}$ cm^{-2}, (c) $\sigma_{3|1,x'x'} = \sigma_{1|2,x''x''} = (0.007 + i0.19)mS, \sigma_{3|1,y'y'} = \sigma_{1|2,y''y''} = (0.001 - i0.14)mS$ for $n = 7 \times 10^{13}$ cm^{-2}, and (d) $\sigma_{3|1,x'x'} = \sigma_{1|2,x''x''} = (0.01 + i0.29)mS$ and $\sigma_{3|1,y'y'} = \sigma_{1|2,y''y''} = (0.002 - i0.12)mS$ for $n = 10 \times 10^{13}$ cm^{-2}. The layer distance is $2d = 5$ nm, and relative orientation between layers is $\theta = 90°$ at 72 THz.

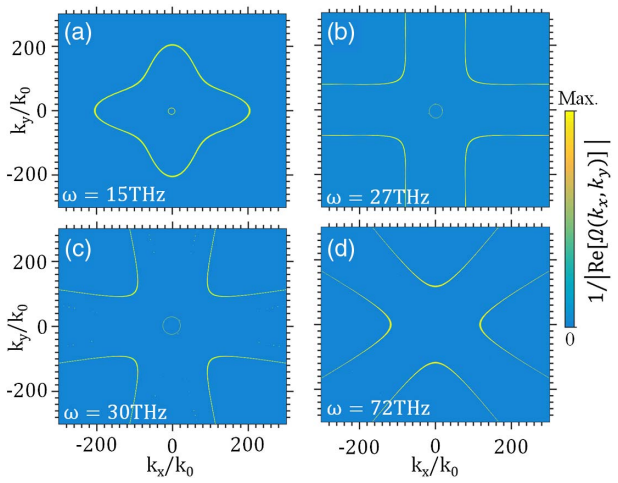

Fig. 5. Transition in the shape of plasmonic modes with varying frequencies. The conductivity values are: (a) $\sigma_{3|1,x'x'} = \sigma_{1|2,x''x''} = (0.06 + i0.41)mS$ and $\sigma_{3|1,y'y'} = \sigma_{1|2,y''y''} = (0.01 + i0.05)mS$, at 15 THz, (b) $\sigma_{3|1,x'x'} = \sigma_{1|2,x''x''} = (0.02 + i0.24)mS$ and $\sigma_{3|1,y'y'} = \sigma_{1|2,y''y''} = (0.004 - i0.008)mS$, at 27 THz, (c) $\sigma_{3|1,x'x'} = \sigma_{1|2,x''x''} = (0.01 + i0.2)mS$ and $\sigma_{3|1,y'y'} = \sigma_{1|2,y''y''} = (0.03 - i0.09)mS$, at 30 THz, and (d) $\sigma_{3|1,x'x'} = \sigma_{1|2,x''x''} = (0.003 + i0.07)mS$ and $\sigma_{3|1,y'y'} = \sigma_{1|2,y''y''} = (0.0006 - i0.16)mS$, at 72 THz. The layer distance is $2d = 5$ nm for $n = 3 \times 10^{13}$ cm^{-2}, and relative orientation is $\theta = 90°$.

conductivity changes from elliptical to hyperbolic at the transition point (~27 THz), there is a change in the shape of the dispersion curve [Figs. 5(b) and 5(c)]. Furthermore, with the increase in conductivity, the shape of the mode changes to a hyperbolic curve. Figure 5(d) shows the dispersion curve for hyperbolic conductivity. These curves show the near-zero transition of anisotropic conductivity from elliptical to hyperbolic regions. The appearance of a central mode in bilayer 2D materials depends on the extent of coupling between layers. For anisotropic material, these modes are present at all rotational angles [27], whereas for hyperbolic material, appearance of these modes depends on the chemical potential and frequency, as shown in Figs. 4 and 5.

In this Letter, we have shown the effect of relative angular orientation and chemical potential on hyperbolic plasmon modes in a bilayer system. It is observed that direction and shape of modes can be modified by rotating one of the layers relative to other. The modes can also be changed by changing the chemical potential of the modes. These tuning parameters can have applications in switches, optoelectronics, and more.

Funding. National Natural Science Foundation of China (NSFC) (11704332, 61574127, 61601408, 61625502, 61775193); Natural Science Foundation of Zhejiang Province (LY17F010008); Top-Notch Young Talents Program of China; Fundamental Research Funds for the Central Universities.

REFERENCES

1. A. Vakil and N. Engheta, Science **332**, 1291 (2011).
2. X. Lin, Y. Yang, N. Rivera, J. J. López, Y. Shen, I. Kaminer, H. Chen, B. Zhang, J. D. Joannopoulos, and M. Soljačić, Proc. Natl. Acad. Sci. USA **114**, 6717 (2017).
3. Z. Jacob and E. E. Narimanov, Appl. Phys. Lett. **93**, 221109 (2008).
4. O. Takayama, A. A. Boydonov, and A. V. Lavrinenka, J. Phys. Condens. Matter **29**, 463001 (2017).
5. F. Xia, H. Wang, and Y. Jia, Nat. Commun. **5**, 4458 (2014).
6. O. Tokayama, P. Dmitriev, E. Shkondin, O. Yermakov, M. Panah, K. Golenitskii, F. Jensen, A. Boydonov, and A. Lavrineno, Semiconductors **52**, 442 (2018).
7. O. Takayama, E. Shkondin, A. Bodganov, M. E. A. Panah, K. Golenitskii, P. Dmitriev, T. Repan, R. Malureanu, P. Belov, F. Jensen, and A. V. Lavrinenko, ACS Photon. **4**, 2899 (2017).
8. Y. Jiang, X. Lin, T. Low, B. Zhang, and H. Chen, Laser Photon. Rev. **12**, 1800049 (2018).
9. W. Ma, Z. Huang, X. Bai, P. Zhan, and Y. Liu, ACS Photon. **4**, 1770 (2017).
10. T. Wu, Y. Luo, and L. Wei, Opt. Lett. **42**, 2066 (2017).
11. C. Qian, X. Lin, Y. Yang, F. Gao, Y. Shen, J. Lopez, I. Kaminer, B. Zhang, E. Li, M. Soljačić, and H. Chen, ACS Photon. **5**, 1506 (2018).
12. X. Shi, X. Lin, I. Kaminer, F. Gao, Z. Yang, J. D. Joannopoulos, M. Soljačić, and B. Zhang, Nat. Phys. **14**, 1001 (2018).
13. P. Li, I. Dolado, F. J. Alfaro-Mozaz, F. Casanova, L. E. Hueso, S. Liu, J. H. Edgar, A. Y. Nikitin, S. Vélez, and R. Hillenbrand, Science **359**, 892 (2018).
14. J. Kang, H. Sahin, H. D. Ozaydin, R. T. Senger, and F. M. Peeters, Phys. Rev. B **92**, 075413 (2015).
15. J. S. Gomez-Diaz, M. Tymchenko, and A. Alù, Phys. Rev. Lett. **114**, 233901 (2015).
16. A. Nemilentsau, T. Low, and G. Hanson, Phys. Rev. Lett. **116**, 066804 (2016).
17. E. Forati, G. W. Hanson, A. B. Yakovlev, and A. Alù, Phys. Rev. B **89**, 081410 (2014).
18. V. P. Drachev, V. A. Podolskiy, and A. V. Kildishev, Opt. Express **21**, 15048 (2013).
19. Y. Ma, C. Shen, A. Zhang, L. Chen, Y. Liu, J. Chen, Q. Liu, Z. Li, M. Amer, T. Nilges, A. N. Abbas, and C. Zhou, ACS Nano **11**, 7126 (2017).
20. M. S. Fuhrer and J. Hone, Nat. Nanotechnol. **8**, 146 (2013).
21. G. Fiori, D. Neumaier, B. N. Szafranek, and G. Iannaccone, IEEE Trans. Electron. Devices **61**, 729 (2014).
22. V. Ryzhii, M. Ryzhii, A. Satou, T. Otsuji, and N. Kirova, J. Appl. Phys. **105**, 104510 (2009).
23. W. J. Yu and X. Duan, Sci. Rep. **3**, 1248 (2013).
24. T. Cao, Z. Li, D. Y. Qiu, and S. G. Louie, Nano Lett. **16**, 5542 (2016).
25. B.-H. Huang, W.-B. Lu, X.-B. Li, J. Wang, and Z.-G. Liu, Appl. Opt. **55**, 5598 (2016).
26. D. Giofré, D. Ceresoli, G. Fratesi, and M. I. Trioni, Phys. Rev. B **93**, 205420 (2016).
27. A. S. Rodin and A. H. C. Neto, Phys. Rev. B **91**, 075422 (2015).
28. E. H. Hwang and S. D. Sarma, Phys. Rev. B **80**, 205405 (2009).
29. J. Ruseckas, G. Juzeliūnas, and I. V. Zozoulenko, Phys. Rev. B **83**, 035403 (2011).
30. L. Jing, Z. Wang, Y. Yang, L. Shen, B. Zheng, F. Gao, H. Wang, E. Li, and H. Chen, IEEE Trans. Antennas Propag. (2018).
31. O. Y. Yermakov, A. I. Ovcharenko, M. Song, A. A. Bogdanov, I. V. Iorsh, and Y. S. Kivshar, Phys. Rev. B **91**, 235423 (2015).
32. O. V. Kotov and Y. E. Lozovik, Phys. Rev. B **96**, 235403 (2017).
33. B. H. Fong, J. S. Colburn, J. J. Ottusch, J. L. Visher, and D. F. Sievenpiper, IEEE Trans. Antennas Propag. **58**, 3212 (2010).
34. O. Y. Yermakov, A. I. Ovcharenko, A. A. Bogdanov, I. V. Iorsh, K. Y. Bliokh, and Y. S. Kivshar, Phys. Rev. B **94**, 075446 (2016).
35. Y. V. Bludov, A. Ferreira, N. M. R. Peres, and M. I. Vasilevskiy, Int. J. Mod. Phys. B **27**, 1341001 (2013).
36. M. Jablan, H. Buljan, and M. Soljačić, Phys. Rev. B **80**, 245435 (2009).
37. J. A. Kong, *Electromagnetic Wave Theory* (Wiley, 1986).